Engineering Journal of Qatar University, Vol. 7, 1994, p. 115 - 134

NUMERICAL STUDY OF MAGNETO-FLUID-MECHANICS FORCED CONVECTION PIPE FLOW

M. J. Al-Khawaja*, R. A. Gardner and R. Agarwal****
*Department of Mechanical Engineering, Qatar University
Doha, Qatar.
**Department of Mechanical Engineering
Washington University, St. Louis, MO 63130-4899, USA.

ABSTRACT

The problem of fully developed, laminar, steady, forced convection heat transfer in an electrically conducting fluid flowing in an electrically insulated, horizontal, circular pipe (whose wall is subjected to a uniform heat flux) in a vertical uniform transverse magnetic field has been considered numerically. The central difference scheme is employed in the analysis. For high Hartmann numbers ($100 \leq M \leq 500$), the refinement of the mesh in the radial direction is necessary in order to handle the effect of the Hartmann boundary layer. To have a convergent solution, under-relaxation is needed for high M. A considerable number of results for MFM forced convection are obtained. All the results (i.e. velocity and temperature distributions and heat transfer), in general, are in a good agreement with the previous work.

NOMENCLATURE

a	Radius of pipe, meter (m)
$\mathbf{B}$	Magnetic flux density vector, tesla (T) = 10^4 gauss
B_0	Uniform magnetic flux, T
B_r, B_ϕ, B_z	Radial, angular and axial magnetic flux, T
B_x	Vertical magnetic flux, T
C_f	Skin coefficient of friction
c	Specific heat, J/kg·°C
d	Diameter of pipe, = $2a$
$\mathbf{E}$	Electric field vector, V/m
E_r, E_ϕ, E_z	Radial, angular and axial electric field, V/m
E_x^*, E_y^*	Dimensionless vertical and horizontal electric field
E_η^*	Dimensionless radial electric field
$\mathbf{F}$	Body force vector, N/m^3
$\mathbf{g}$	Gravitational acceleration vector, m/s^2

g	Downward gravitational acceleration, m/s^2
g_r, g_ϕ, g_z	Components of gravitational acceleration in r, ϕ and z-directions, m/s^2
h	Mesh size in η-direction
h_c	Heat-transfer coefficient, w/m$^2\cdot$°C
$\mathbf{H}$	Magnetic field vector, A/m
H	Dimensionless induced axial magnetic field, $H_z/[u_m(\sigma\mu_f)^{1/2}]$
$H_{\hat{}Xx\hat{}HH\phi}$,H_z	Dimensionless radial, angular and axial magnetic field
H^*	Normalized magnetic field, H/γ
i	Integer variable in η-direction, 1,2,3,....,$L-1$
$\mathbf{J}$	Electric current density vector, A/m^2
j	Integer variable in ϕ-direction, 0,1,2,3,....,K
K	Maximum of j, integer at where $\phi = \pi/2$
k	Thermal conductivity of fluid, w/m$\cdot$°C
L	Maximum of i, integer where $\eta = 1$
M	Hartmann number, $B_0 a(\sigma/\mu_f)^{1/2}$
n	Iteration step number, integer 1,2,3,....
Nu	Nusselt number, $h_c d/k$
p	Fluid pressure, N/m^2
Pr	Prandtl number, $c\mu_f/k$
q	Constant heat flux, $-q_w$
q_w	Constant wall heat flux, w/m^2
r	Radial coordinate measured from the centerline of pipe, m
R_M	Magnetic Reynlods number, $\sigma\mu u_m a$
R_s	Root-mean square residuals for the variable s, defined in (4.1)
s	Fluid property
S	Sensitivity, defined in Reference [8]
T	Temperature, °C
T_m	Bulk mean temperature, °C
ΔT	Temperature difference, °C
$\mathbf{u}$	Velocity vector, m/s
u_m	Mean axial velocity, m/s
u_z	Axial fluid velocity, m/s
w	Dimensionless axial velocity, u_z/u_m
w^*	Normalized axial velocity, w/γ
x	x-coordinate, m
x^*	Dimensionless x-coordinate, x/a
y	y-coordinate, m
y^*	Dimensionless y-coordinate, y/a
z	Axial coordinate, m

Greek Letters

γ	Non-dimensional pressure gradient, $[(\partial p/\partial z)(a^2)]/u_m\mu_f$
$\delta\phi$	Mesh size in ϕ-direction, radiant
∇^2	Laplacian in dimensionless cylindrical coordinate unless stated otherwise
η	Dimensionless radial coordinate, r/a
θ	Dimensionless temperature, $(T-T_a)/(aq/k)$
μ	Magnetic permeability of fluid, H/m
μ_f	Dynamic viscosity of fluid, N·s/m^2
ν	Kinematic viscosity of fluid, m^2/s
ρ	Density of fluid, kg/m^3
σ	Electrical conductivity of fluid, A/V·m
ϕ	Angular coordinate measured from direction of magnetic field, radiant
ω	Relaxation parameter

Subscripts

c	Refers to centerline of pipe
f	Refers to friction
i	Refers to the radial discretization
j	Refers to the angular discretization
M	Refers to magnet
m	Refers to mean
r, ϕ, z	Refers to components in r, ϕ and z-directions
η, x, y	Refers to components in η, x and y-directions
w	Refers to wall

Superscripts

n	Refers to iteration step

INTRODUCTION

MFM forced convection through a circular pipe with and without heat transfer is very attractive problem. Hartmann, [6], obtained the exact solution of the flow between two parallel, non-conducting walls with the applied magnetic field normal to the walls. Shercliff, [7], solved the problem of rectangular duct, from which he noticed that for high Hartmann numbers M the velocity distribution consists of a uniform core with a boundary layer near the walls. This result enabled him to solve the problem for a circular pipe in an approximate manner (a first

approximation which gives rise to errors of order M^{-1}) for large M assuming walls of zero conductivity and, subsequently, walls with small conductivity (Shercliff, [8]). Chang & Lundgren, [9], considered the effect of wall conductivity for this problem. Gold, [10], analytically solved the MHD problem in a circular pipe with zero wall conductivity. His solution was an infinite series of Bessel functions, which was approximated for large M with the first few terms. For the same problem, Shercliff, [11], used the second approximation (which gives rise to errors of order M^{-2}) to get the solution for large M. Gardner, [12], used Gold's solution to evaluate the exact solution for temperature profile, which turned out to be very complex. Then, he approximated velocity profile for small to moderate M with a polynomial form from which he calculated the Nusselt number Nu. For large M, he used Gold's approximation to determine Nu. In the present work, we solve this problem numerically using central difference second-order accurate scheme with Gauss-Seidel SOR iteration methods to obtain dimensionless axial velocity w, Induced magnetic field H, and temperature θ from which we calculate dimensionless pressure gradient and local and average Nusselt numbers and compare them with the previous results. Those results are for special case, which help us t^Xxadvance in^Xx more general one of combined free and forced convection of MFM pipe flow. In this special problem, we should regard the vertical and the horizontal coordinates as the lines of the symmetry. Thus, we would consider only one quadrant of the circle given in Figure 1. We should

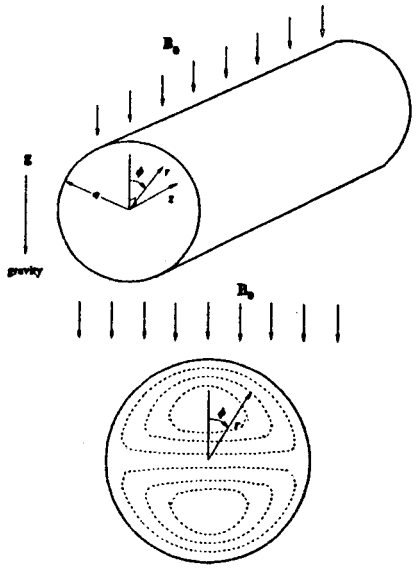

Fig. 1: Pipe cross section showing coordinate system and induced electric current lines, [3]

notice that H is asymmetric along the horizontal line, but this does not cause a problem since the horizontal line simply reflects the negative value of H.

GOVERNING EQUATIONS

Referring to Figure 1 and from the assumptions that the flow is laminar, steady, fully developed in an electrically conducting fluid flowing in an electrically insulated, horizontal, circular pipe whose wall is subjected to a uniform heat flux in a uniform transverse magnetic field, the dimensionless governing equations for forced convection MFM pipe flow under transverse magnetic field can be written as, [1], (To derive those equations, a major assumption has been made, that is, the magnetic Reynolds number has been assumed to be very small compared to the unity. This will make the induced fields much smaller than the total or the applied field. Accordingly the governing equations would be simplified very significantly. Consult Reference [1] for more details).

$$\nabla^2 H^* + M\left(\frac{\sin\phi}{\eta}\frac{\partial w^*}{\partial \phi} - \cos\phi\frac{\partial w^*}{\partial \eta}\right) = 0 \tag{1}$$

$$\nabla^2 w^* + M\left(\frac{\sin\phi}{\eta}\frac{\partial H^*}{\partial \phi} - \cos\phi\frac{\partial H^*}{\partial \eta}\right) = 1 \tag{2}$$

and

$$\nabla^2\theta \downarrow \tag{3}$$

where the Laplacian ∇^2 operator is given by

$$\nabla^2 = \frac{\partial^2}{\partial \eta^2} + \frac{1}{\eta}\frac{\partial}{\partial \eta} + \frac{1}{\eta^2}\frac{\partial^2}{\partial \phi^2}$$

and where the dimensionless velocity w and the axial velocity is related by $w = u_z/u_m$ and the normalized velocity is defined as $w^* = w/\gamma$. The boundary conditions can be stated as following:

$$\left.\begin{aligned} w \mid_{\eta=1} &= 0 \\ v \mid_{\eta=1} &= -\frac{\partial \psi}{\partial \eta} \mid_{\eta=1} = 0 \end{aligned}\right\} \quad \text{from no-slip condition,}$$

$$u \mid_{\eta=1} = \frac{1}{\eta}\frac{\partial \psi}{\partial \phi} \mid_{\eta=1} = 0 \qquad \text{from impermeable condition.}$$

From which, one can deduce that it is sufficient to let

$$\psi \mid_{\eta=1} = 0$$

Beside,

$$H \mid_{\eta=1} = 0 \qquad \text{from zero wall conductivity,}$$

$$\frac{\partial \theta}{\partial \eta} \mid_{\eta=1} = 1 \qquad \text{from uniform heat flux .}$$

DIFFERENCE EQUATIONS

Equations (1) to (3) can be discretized by utilizing the central difference scheme to obtain the following difference equations,

$$G_1 w^*_{i+1,j} + G_2 w^*_{i-1,j} + G_3 w^*_{i,j+1} + G_3 w^*_{i,j-1} + G_0 w^*_{i,j} = C_{i,j} \qquad (4)$$

$$G_1 H^*_{i+1,j} + G_2 H^*_{i-1,j} + G_3 H^*_{i,j+1} + G_3 H^*_{i,j-1} + G_0 H^*_{i,j} = D_{i,j} \qquad (5)$$

and

$$G_1\theta_{i+1,j} + G_2\theta_{i-1,j} + G_3\theta_{i,j+1} + G_3\theta_{i,j-1} + G_0\theta_{i,j} = -^2 h^2 w_{i,j} \qquad (6)$$

where

$$G_1 = 1 + \frac{1}{2i} \;,\quad G_2 = 1 - \frac{1}{2i} \;,\quad G_3 = \frac{1}{(i\delta\phi)^2} \;,\quad G_0 = -2[1 + \frac{1}{(i\delta\phi)^2}]$$

$$C_{i,j} = h^2\gamma - \frac{hM}{2}[\frac{\sin(j\delta\phi)}{i\delta\phi}\,\bar{\delta}_\phi H^*_{i,j} - \cos(j\delta\phi)\,\bar{\delta}_\eta H^*_{i,j}]$$

$$D_{i,j} = -\frac{Mh}{2}\left[\frac{\sin(j\delta\phi)}{i\delta\phi}\,\bar{\delta}_\phi\, w^*_{i,j} - \cos(j\delta\phi)\,\bar{\delta}_\eta\, w^*_{i,j}\right]$$

and

$$\bar{\delta}_\eta(\,)_{i,j} = (\,)_{i+1,j} - (\,)_{i-1,j} \;,\quad \bar{\delta}_\phi(\,)_{i,j} = (\,)_{i,j+1} - (\,)_{i,j-1}$$

SOLUTION OF THE EQUATIONS

The systems of linear algebraic equations can be solved by employing point-Gauss-Seidel iterative method and this procedure can be summarized as following,

1) construct initial distribution for H^*, w^*, and θ,
2) compute the variables at the center using the rectangular form of the finite difference equations for next iteration,
3) apply Dirichlet boundary conditions for the velocity and the induced magnetic field,
4) apply symmetric conditions along the vertical line and horizontal line, and compute the variables at $\phi = -\delta\phi$ for next iterative cycle and calculate the variables at $\phi = \pi/2+\delta\phi$ for the present iteration,
5) advance the equations for the variables 1-cycle using Eqns. (4), (5), and (6) and apply Gauss-Seidel method,
6) apply Neumann boundary condition for temperature,
7) check the convergence by testing root-mean-square residuals R_s for each flow

variable. Convergence is considered to be achieved when $R_s < 10^{-4}$. R_s is defined as,

$$R_s = \sqrt{\sum_{i=0}^{L}\sum_{j=0}^{K}(s_{ij}^{n+1} - s_{ij}^{n})^2} \qquad (7)$$

8) repeat steps 2)-7) until convergence is achieved.

RESULTS

Some numerical results obtained for the case of MFM forced convection laminar pipe flow in a transverse magnetic field with heat transfer, which could be helpful in handling the problem when the free convection is added, are found to be in good agreement with Gold's exact solution, [10], and Gardner's approximate solution, [12].

In this computation, only one quadrant is considered since this problem is symmetrical along the vertical and horizontal diameters. The SOR (successive over relaxation) is utilized to accelerate the iterations with $\omega = 1.2$, (All relaxation parameters ω given here are only for w^* and H^* but $\omega = 0.8$ for θ is used in all computations for since the boundary condition for θ is Neumann type and it would introduce more error. Consequently, there would be some stability problem in using line-iterative method for solving θ for $\omega > 0.8$. Therefore, it is preferable to let $\omega = 0.8$ for θ to make the solution more stable.) and this is used only for low and moderate M at 24×12 grid, but for high M, SUR (successive over relaxation) must be employed to decelerate the iterations. As an example, for $M = 100$ and for $M = 500$ at the same mesh size, $\omega = 0.7$ and $\omega = 0.18$ should be selected, respectively. The reason for using SUR is due to the source terms. Refining the mesh also would solve part of this problem, for example, when 124×12 mesh is used the relaxation parameter ω for $M = 100$ and $M = 500$ would be increased to 1.0 and 0.6, respectively.

If R_{H^*}, R_{w^*} and R_θ are the root-mean-square residuals [defined in Eqn.(7)] for H^*, w^* and θ, respectively, it can be noticed through the results obtained that at, 24×12 mesh, R_{H^*} and R_{w^*} would converge faster than R_θ, and this difference becomes more apparent for high M at $124\times$ 12 mesh. As an example, for low M, R_{H^*} and R_{w^*} would reach almost a value of zero but R_θ would reach a value of 5×10^{-4} after 1,500 iterations (See Figure 2a). For high M (100 to 500), R_{H^*} and R_{w^*}

would reach a value of 10^{-8} after 1,800 iterations, in contrast to R_θ which would reach a value of 6×10^{-4} after 4,300 iterations (See Figure 2b).

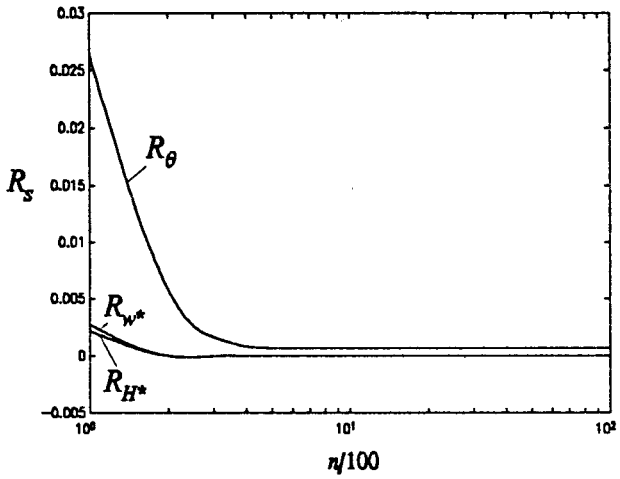

Figure 2a. Root-mean-square residuals R_s vs. number of iterations n per 100 iterations for low M (=10)

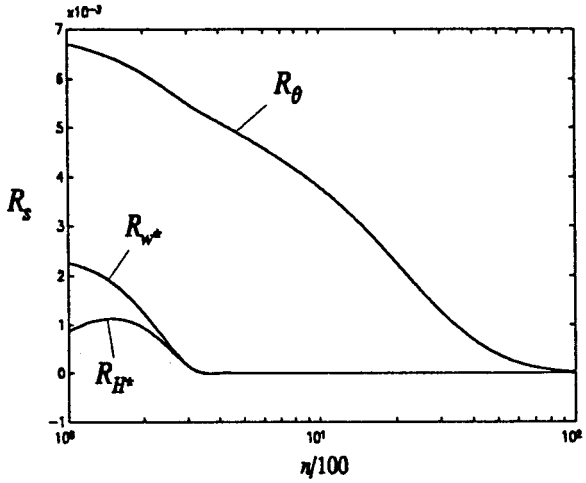

Figure 2b. Root-mean-square residuals R_s vs. number of iterations n per 100 iterations for high M (=10)

Now, some of the plots obtained for MFM forced convection pipe flow will be discussed and will be compared with the previous work, [10] and [12]. Figure 3 shows the profiles of the normalized axial velocity profiles as a function of η for

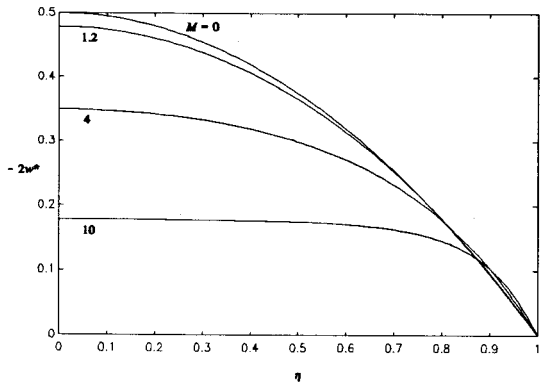

Figure 3. Normalized velocity profiles plot along the radial direction at different low Hartmann numbers M and at $\phi = 0$

low M (1.2 to 10) at $\phi = 0$. You can notice that the profiles would tend to be flattened as M increases. This flattening becomes clear for large M and the velocity w profiles, as seen in Figure 4, become uniform along the radial direction at zero

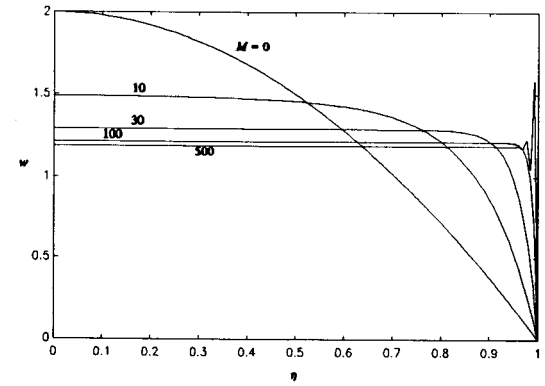

Figure 4. Dimensionless velocity profiles along the radial direction as a function of Hartmann numbers M at $\phi = 0$

angle from the field. For an angle of 90° from the field the velocity profiles seem to have less flattening and tend to preserve the parabolic shape as seen in Figure 5. The reason for this is that at $\phi = 90°$ and near the boundary, J_r would tend to

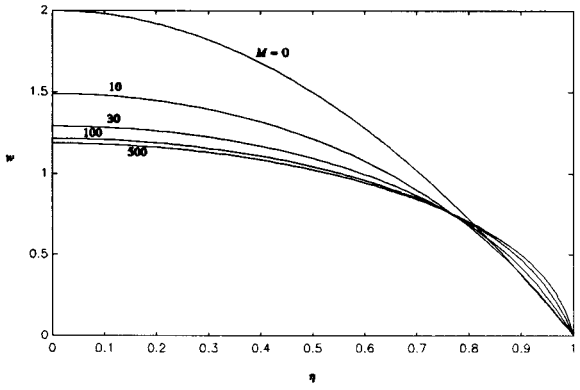

Figure 5. Dimensionless velocity profiles along the radial direction as a function of Hartmann numbers M at $\phi = \pi/2$

vanish since the wall is electrically non-conducting and the other current density component J_ϕ does not interact with B_0 since they are parallel. Therefore, one expects the ponderomotive force tends to vanish at that region. At $\phi = 0$, the Hartmann boundary layer develops at high M and the solution oscillates near the boundary. Figure 4 shows these oscillations near the boundary at $\phi = 0$ and they become noticeable at $M = 500$ for 124×12 mesh. Those oscillations could be damped out by refining the mesh along the radial direction particularly near Hartmann boundary layer. Figures 6 and 7 show a good agreement between the numerical normalized velocity profiles and Gold's exact and asymptotic solutions for $M = 10$ and $M = 100$, respectively, at $\phi = 0°$ and 90°. Also, the numerical result for negative non-dimensional axial pressure gradient $-\gamma$ as a function of M agrees with that obtained exactly or asymptotically. See Figures 8 and 9. As M gets higher, in Figure 9, the relation between $-\gamma$ and M becomes linear (straight line) with a slope of $3\pi M/8$ as it was predicted by Shercliff, [8]. The numerical result for the normalized induced magnetic field is plotted as η for $M = 4$ and $M = 10$ at $\phi = 0$ and a good agreement with Gold's solution is obtained in Figure 10. Figure 11 shows the dimensionless radial electric field profiles along the horizontal radius, $\phi = \pi/2$, for different values of Hartmann numbers. Those profiles behave in similar way as velocity profiles shown in Figure 5. Figure 12 compares the sensitivity S defined in Reference [8] with Gold's solution. The

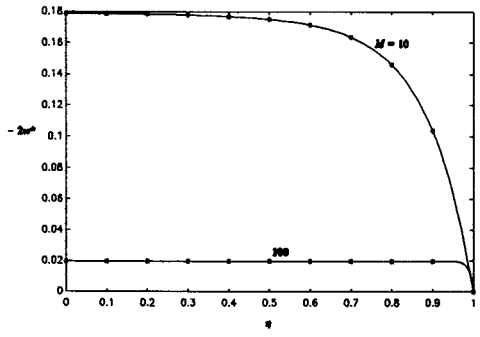

Figure 6. Comparison of numerical data of normalized velocity profiles at $\phi = 0$ with Gold's solution, [10]. *, Gold's solution; ——, Present work

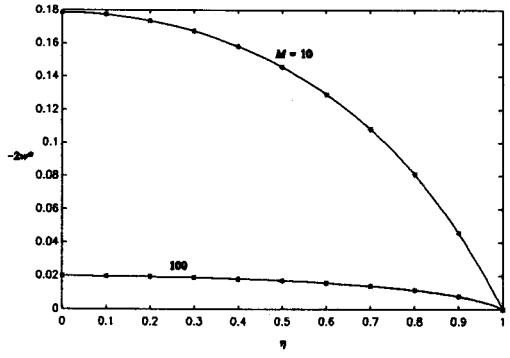

Figure 7. Normalized velocity profiles at $\phi = \pi/2$. *, Gold's solution; ——, [10], Present work

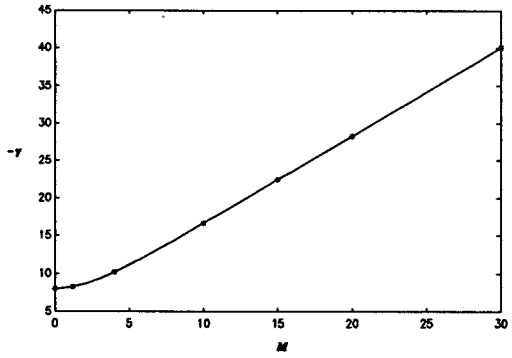

Figure 8. Relations between negative non-dimensional pressure gradient $-\gamma$ and low to moderate Hartmann numbers. *, Gold's solution; ——, [10], Present work

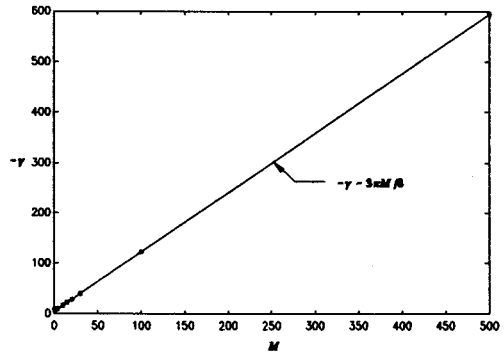

Figure 9. Relations between negative non-dimensional pressure gradient $-\gamma$ and low and high Hartmann numbers. *, Gold's solution; ——, [10], Present work

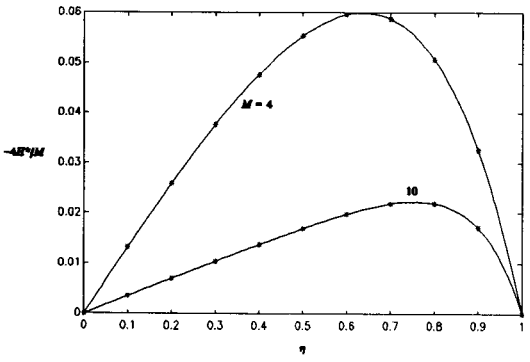

Figure 10. Normalized induced magnetic field along the radial direction at $\phi = 0$. *, Gold's solution; ——, [10], Present work

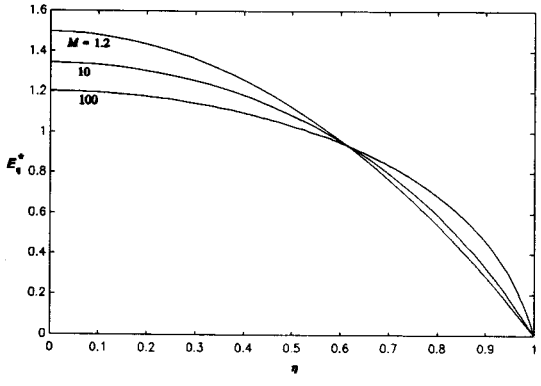

Figure 11. Dimensionless radial electrical field along the horizontal radius, $\phi = \pi/2$, for different values of M

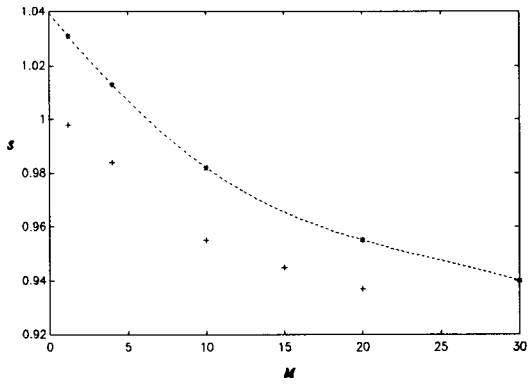

Figure 12. Sensitivity *vs*. Hartmann number M. *, present work; +, Gold's solution, [10]

present numerical solution has a slight deviation for low M but for high M ($\sim$ 100 not shown in the figure), the asymptotic Gold's solution for sensitivity ($S = 0.925$) is almost identical to the present numerical solution which is 0.928. Figure 13

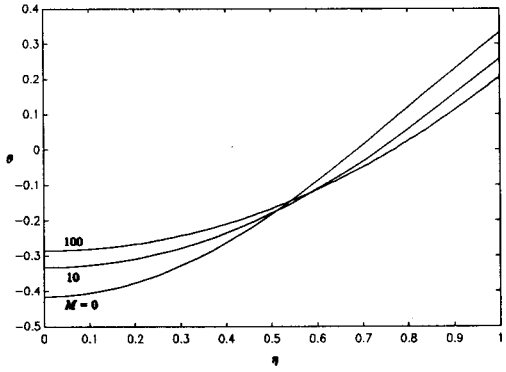

Figure 13. Dimensionless temperature profiles along the radial direction at $\phi = 0$ at different values of Hartmann numbers M

depicts the temperature profiles at $\phi = 0$ where they tend to flatten and approach a constant value as M increases, but this effect would be less at $\phi = 90°$. See Figure 14. The explanation of this is that the velocity profiles are more flattened

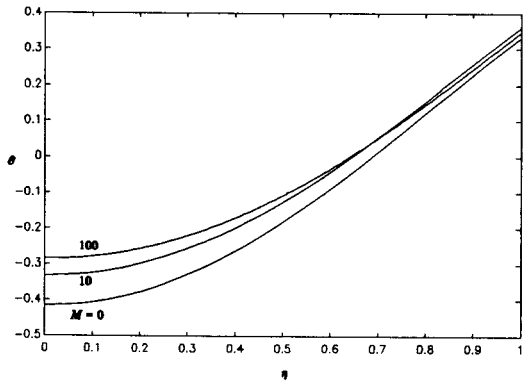

Figure 14. Dimensionless temperature profiles along the radial direction at $\phi = \pi/2$ for different values of Hartmann numbers M

near $\phi = 0$ from those near $\phi = 90°$. Furthermore, Nu can be plotted as a function of ϕ (since θ_w depends on ϕ) for different values of M as shown in Figure 15. At $M = 0$, Nu has a constant value which is very close to 48/11 as in the case

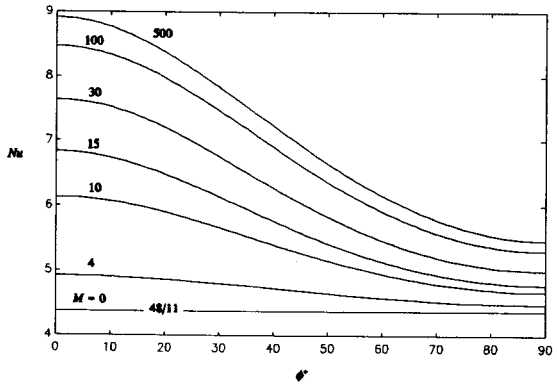

Figure 15. Local Nusselt number as a function of the angular coordinate measured from the direction of the magnetic field

of the absence of the magnetic field. As M increases, Nu increases and approaches the value 8 at $\phi = 0$ as in the case for uniform velocity profile in pipe flow. See Figure 15. Figure 16 shows a good agreement with Gardner's approximate solution

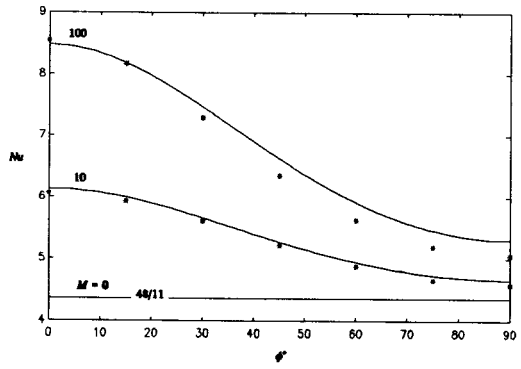

Figure 16. Comparison of numerical data of local Nusselt number with Gardner's approximation, [12]. *, Gardner's solution; ——, Present work

for Nu at low and high M. Figure 17 compares the numerical data for the average

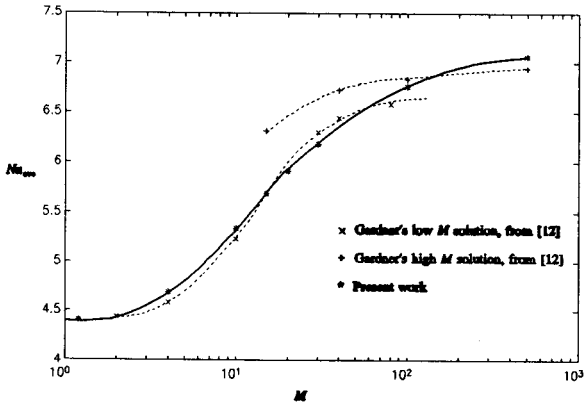

Figure 17. Average Nusselt number as a function of M

Nusselt number as a function of M with Gardner's approximations for both high and low M. As before, there is a close agreement. Finally, Figure 18 can be compared with the result obtained by Gardner, [12], for MFM forced convection where the velocity profiles flatten as M increases and the flattening is more pronounced at $\phi = 0, \pi$.

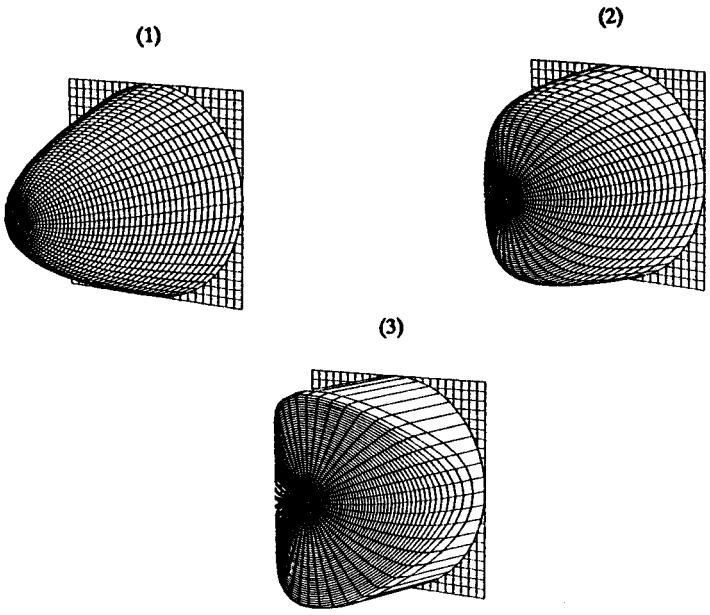

Figure 18. Axial velocity w profiles for MFM forced convection, $M = 0$ and $Pr = 0.024$. (1), $M = 0$; (2), $M = 10$; (3), $M = 100$

CONCLUSIONS

In conclusion, one can notice that the numerical results are, in general, in a good agreement with the literature. In MFM forced convection flow, the numerical results are almost identical to Gold's solution, [10], and Gardner's approximation, [12]. In this case, the problem of the Hartmann boundary layer at large M could be resolved by refining the mesh near the boundary in the radial direction. The source terms discussed in Reference [1] would cause the solution to diverge at high M, but refining the mesh in radial and angular directions or under-relaxing the line-iterative scheme, the solution would converge even for high M.

REFERENCES

1. **Al-Khawaja, M. J., Gardner, R. A., Agarwal, R., 1992.** "Numerical Study of MFM Free-and-Forced convection Pipe Flow", Ph. D. Dissertation, Washington University, St. Louis, MO.

2. **Branover, H., 1978.** "Magnetohydrodynamic Flow in Ducts", Keter Publishing House Jerusalem Ltd., Jerusalem.

3. **Lo, Y. T., 1973.** "Combined free-and-forced convection in a Transverse Magnetic Field", M.S. Thesis, Washington University, St. Louis, MO.

4. **Williams, E. J., 1930.** "The Induction of EMF's in a Moving Fluid by a Magnetic Field and Its Application to an Investigation of the Flow of Liquids", Proc. Phys. Soc., Vol. 42, p. 466.

5. **Hartmann, J. and Lazarus, F., 1937.** "Hg-Dynamics II", Math-Fys. Medd., Vol. 15, No. 7.

6. **Hartmann, J., 1937.** "Hg-Dynamics I", Math-Fys. Medd., Vol. 15, No.

7. **Shercliff, J. A., 1953.** "Steady Motion of Conducting Fluids in Pipes under Transverse Magnetic Field", Proc. Cambr. Phil. Soc., Vol. 49, pp. 126-144.

8. **Shercliff, J. A., 1956.** "The Flow of Conducting Fluids in Circular Pipes under Transverse Magnetic Field", J. Fluid Mech., Vol. 1, p. 644.

9. **Chang, C. C. and Lundgren, T. S., 1961.** "Duct Flow in Magnetohydrodynamics", ZAMP, Vol. 12, No. 2, p. 100.

10. **Gold, R., 1962.** "Magnetohydrodynamic Pipe Flow", Part 1, J. Fluid Mech., Vol. 13, p. 505.

11. **Shercilff, J. A., 1962.** "Magnetohydrodynamic Pipe Flow", part 2 High Hartmann Number, J. Fluid Mech., Vol. 13, p. 513.

12. **Gardner, R. A., 1968.** "Laminar Pipe Flow in a Transverse Magnetic Field with Heat Transfer", Int. J. Heat Mass Transfer", Vol. 11, pp. 1076-1081.

13. **Ozisik, M. N., 1980.** "Heat Conduction", John Wiley & Sons, Inc., New York.

14. **Hughes, W. F. and Young, F. J., 1966.** "The Electromagnetodynamics of Fluids", John Wiley & Sons, Inc., New York.

15. **Smith, G. D., 1985.** "Numerical Solution of Partial Differential Equations", Third Edition, Clarendon Press, Oxford.

16. **Woods, L. C., 1954.** "A note on the Numerical Solution of Fourth Order Differential equations", Aeronautics Quarterly, Vol. 5, p. 176.